International Journal of
Molecular Sciences

MDPI

Article

Expression and Membranous Localization of CD44 Define Distinct Cellular and Spatial Phenotypes Associated with Glioma Aggressiveness

Carola N. Jaunecker [1,2], Laura Kerschbaumer [2,3], Valérie Quinot [4], Julia Freund [2,3,5,6], Leah Mager [2,5,6], Sarah Machreich [2,5,6], Linda Pacher [2,3], Katharina Bruckner [2,5,6], Laura Marosits [2,3], Bernhard Robl [2,5,6], Alexandra Lang [2,3], Lisa Gabler-Pamer [2,3], Dominik Kirchhofer [1,2], Christine Pirker [1,2], Karl Rössler [2,3], Anna S. Berghoff [7], Barbara Kiesel [2,3], Georg Widhalm [2,3], Thomas Roetzer-Pejrimovsky [2,4], Walter Berger [1,2] and Daniela Lötsch [2,3,*]

1 Center for Cancer Research, Medical University of Vienna, Borschkegasse 8a, 1090 Vienna, Austria
2 Comprehensive Cancer Center, Medical University & General Hospital, Waehringer Guertel 18-20, 1090 Vienna, Austria
3 Department of Neurosurgery, Medical University of Vienna, Waehringer Guertel 18-20, 1090 Vienna, Austria
4 Department of Neurology, Division of Neuropathology and Neurochemistry, Medical University of Vienna, Waehringer Guertel 18-20, 1090 Vienna, Austria
5 Department of Pediatrics and Adolescent Medicine, Medical University of Vienna, Waehringer Guertel 18-20, 1090 Vienna, Austria
6 Comprehensive Center for Pediatrics, Medical University & General Hospital, Waehringer Guertel 18-20, 1090 Vienna, Austria
7 Division of Oncology, Department of Medicine I, Medical University of Vienna, Waehringer Guertel 18-20, 1090 Vienna, Austria
* Correspondence: daniela.loetsch@meduniwien.ac.at

Abstract

Adult-type diffuse gliomas comprise, amongst others, biologically distinct isocitrate dehydrogenase (IDH)-mutant (IDH-MUT) astrocytomas and IDH-wildtype (IDH-WT) glioblastoma (GB). Although IDH-MUT astrocytomas generally have a more favorable prognosis, they frequently recur and progress. Despite extensive molecular characterization, key drivers of glioma progression remain elusive. CD44, a hyaluronic acid receptor, has been implicated in glioma invasion and progression. We investigated CD44 expression, localization, and spatial organization across IDH-WT GB and IDH-MUT astrocytomas and their association with tumor progression and cellular states. CD44 expression and localization were assessed in IDH-WT ($n = 15$) and IDH-MUT ($n = 17$) diffuse gliomas across WHO grades by immunohistochemistry (IHC). Multiplex IHC combined with AI-assisted digital pathology (HALO) evaluated associations between CD44, GFAP-positive astrocytic, and NeuN/*RBFOX3*-positive neuronal regions. Findings were validated using independent snRNA-seq data. IDH-WT GB exhibited significantly higher CD44 expression with prominent membranous localization. Lower-grade IDH-MUT astrocytomas showed reduced, diffuse staining, whereas higher-grade tumors acquired a membranous CD44 localization, resembling IDH-WT GB. CD44 was strongly associated with GFAP-positive astrocytic regions and inversely correlated with NeuN/*RBFOX3*-positive neuronal areas in IDH-MUT tumors. AI-assisted spatial analyses confirmed distinct CD44-positive astrocytic and NeuN-positive neuronal niches, supported by snRNA-seq demonstrating positive *CD44-GFAP* correlations. This association was strongest in astrocytic (AC-like) metaprograms of WHO grade 2, while in higher-grade tumors it was more pronounced in mesenchymal (MES-like) states. CD44 exhibits IDH- and grade-dependent spatial patterns marking glioma progression and astrocytic/mesenchymal tumor states. Membranous CD44 acquisition

Check for updates

Academic Editor: Lorenzo Corsi

Received: 15 October 2026
Revised: 5 November 2026
Accepted: 6 November 2026
Published: 11 November 2026

Copyright: © 2026 by the authors. Licensee MDPI, Basel, Switzerland. This article is an open access article distributed under the terms and conditions of the Creative Commons Attribution (CC BY) license.

accompanies progression to higher grades in IDH-MUT astrocytomas, suggesting CD44 as a marker of glioma aggressiveness.

Keywords: glioma; CD44; progression; spatial organization

1. Introduction

Adult-type diffuse gliomas account for the most common primary brain tumors in adults, with a prognosis strongly varying based on the tumor subtype. Presumably arising from neuronal stem cells and glial progenitor cells, gliomas are a highly heterogeneous group encompassing astrocytoma, oligodendroglioma, as well as the highly aggressive subtype glioblastoma (GB) [1,2].

Based on histological appearance and cell morphology, diffuse gliomas are categorized into WHO grades 2–4, with grade 2 usually accounting for less aggressive low-grade gliomas (LGGs) associated with low mitotic activity. High-grade gliomas (HGGs) are assigned to WHO grade 3 or 4, with GB representing the most aggressive form in adult patients [3]. However, as classification solely based on histopathological characteristics often remains inconclusive and does not provide any information on possible therapeutic options, great effort has been dedicated to the molecular classification of these tumors, identifying characteristic mutations or alterations for each tumor subtype [4]. Thus, tumor classification initially based on gene expression patterns [5] and later defined by DNA methylation profiling has emerged as a valuable tool in brain tumor diagnostics. In this context, the Molecular Neuropathology (MNP) classifier [6] enables the distinction of several methylation subclasses of adult-type diffuse glioma, including GB receptor tyrosine kinase subgroups 1 (RTK1) and RTK2 as well as mesenchymal (MES). Broadly, the RTK1, RTK2, and MES methylation subclass correspond to the proneural, classical and mesenchymal transcriptional subtypes, respectively, as originally defined by Verhaak [5]. With respect to isocitrate dehydrogenase (IDH)-mutant astrocytoma, the MNP classifier further distinguishes low-grade (IDH_LG) and high-grade (IDH_HG) methylation subclasses, which differ markedly in cellular composition, gene expression profiles, patient age, and clinical outcome [7,8]. However, as these methylation profiles may shift between subclasses during glioma progression, there is a need for additional robust markers that capture glioma aggressiveness and progression beyond epigenetic subclassification [7].

One central molecular marker for characterization of glioma is the mutation status of the metabolic enzyme IDH, which can either be mutated (IDH-MUT) in the cases of oligodendroglioma or astrocytoma, or wildtype (IDH-WT) in the case of GB. Mutation of IDH results in reduction of α-ketoglutarate to the oncometabolite 2-hydroxyglutarate (2HG), leading to increased sensitivity to oxidative damage and DNA hypermethylation by inhibition of DNA demethylases [9–11]. Considering their central role in glioma, several IDH inhibitors targeting the mutant form of IDH1 and IDH2 have been developed and clinically approved [12]. However, the efficacy of IDH inhibition, for example, by Vorasidenib, and its impact on overall survival in HGG are critically discussed [12–14].

In addition to metabolic alterations, mutations of epidermal growth factor receptor (*EGFR*), promoter mutations affecting the expression of the telomerase reverse transcriptase (*TERT*), or promoter methylation of the O^6-methylguanine-DNA methyltransferase (*MGMT*) are prominent prognostic and predictive markers for glioma [15].

Although huge efforts have been dedicated towards the development of novel targeted treatment approaches for glioma, efficacy of novel therapies remains low, caused by ineffective drug delivery through the blood–brain barrier or the highly heterogeneous tumor cell populations leading to resistance development and high recurrence rates [16,17].

Beyond tumor cell communication, the interaction between tumors cells and the surrounding microenvironment contributes substantially to the highly invasive and therapy-refractory phenotype of diffuse gliomas [18]. Among the key mediators of these interactions is CD44, a transmembrane glycoprotein frequently enriched in glioma tissue [19], that functions as a major adhesion receptor for extracellular matrix (ECM) components including hyaluronic acid [20]. Through its extracellular ligand binding- and intracellular signaling domain, CD44 mediates cell–ECM interactions and influences cellular adhesion, migration and invasion [21,22]. In addition to its membrane-bound form, CD44 can undergo proteolytic cleavage releasing a soluble extracellular domain [23]. Recent studies have further identified CD44 as a hypoxia-induced mesenchymal-associated marker linked to specific cellular metaprograms, where it contributes to enhanced proliferation and invasion [24]. Although CD44 has emerged as potential therapeutic target [22], reflecting its functional involvement in aggressive tumor cell states, its biological and clinical relevance across molecularly distinct glioma subtypes remains incompletely understood. In particular, whether overall CD44 expression or rather its subcellular localization and spatial distribution better reflect tumor aggressiveness or tumor progression has not been sufficiently explored. Addressing this gap is particularly relevant given the limited therapeutic options for patients with higher-grade IDH-MUT astrocytomas [25] and IDH-WT GBs [26], which largely rely on radio/chemotherapy, highlighting the need to identify additional molecular markers of tumor progression and potential therapeutic vulnerabilities. Therefore, in this study, we comprehensively characterized spatial differences in CD44 expression between IDH-WT GB and IDH-MUT astrocytoma and evaluated its association with molecular markers and clinical parameters linked to glioma aggressiveness.

2. Results

2.1. CD44 Is Significantly Enriched in Membranous Regions of IDH WT Glioma

Given the ongoing debate regarding the role of CD44 in glioma aggressiveness, invasiveness, and cellular plasticity, we aimed to investigate differences in CD44 protein expression between IDH-WT GBs ($n = 15$) and IDH-MUT astrocytomas ($n = 17$) and assessed its relationship with established markers of tumor aggressiveness and cellular differentiation. Importantly, CD44-positive cells were significantly enriched in IDH-WT GB compared to IDH-MUT astrocytoma (Figure 1A), reflected by higher staining intensity (Figure 1B). In addition, distinct differences regarding the distribution of strong, moderate, and weak CD44 expression were observed between IDH-WT GB and IDH-MUT astrocytoma (Figure 1C). Regarding cellular localization of CD44, we observed a membrane-specific enrichment in IDH-WT gliomas ($n = 7$), whereas it was more diffusely distributed in cells of IDH-MUT astrocytoma ($n = 13$) (Figure 1D). This significantly elevated membrane-specific localization of CD44 in IDH-WT GB was confirmed by AI-assisted quantification of membranous staining (Figure 1E).

Besides automated HALO-based evaluation of CD44 immunoreactivity, a neuropathological assessment of tumor tissue and adjacent brain parenchyma was performed. In line with AI-assisted analysis, neoplastic cells in IDH-WT GB exhibited strong membranous CD44 staining. A comparable pattern was observed in WHO grade 4 IDH-MUT astrocytomas, while tumor cells of WHO grade 2 or 3 were largely CD44-negative or showed only weak, diffuse immunoreactivity (Figure 1D, lower panels; and Figure 2E, lower panel). When examining CNS tissue adjacent to tumorigenic regions in IDH-MUT astrocytomas, we observed CD44 positivity of tumor cells infiltrating CNS tissue (tumor infiltration zone) (Figure 1F, first column; Supplementary Figure S1A) as well as in astroglial cells of subpial and perivascular regions (Figure 1F, second column; Supplementary Figure S1B,C). In addition, a diffuse, fine granular CD44 staining was observed in the surrounding CNS

white matter, potentially reflecting reactive gliosis (Figure 1F, third column). All of these different regions were partially infiltrated by IDH-mutant glioma cells (Figure 1F, middle row), indicating that CD44 positivity may, at least in part, reflect the presence of infiltrating tumor cells.

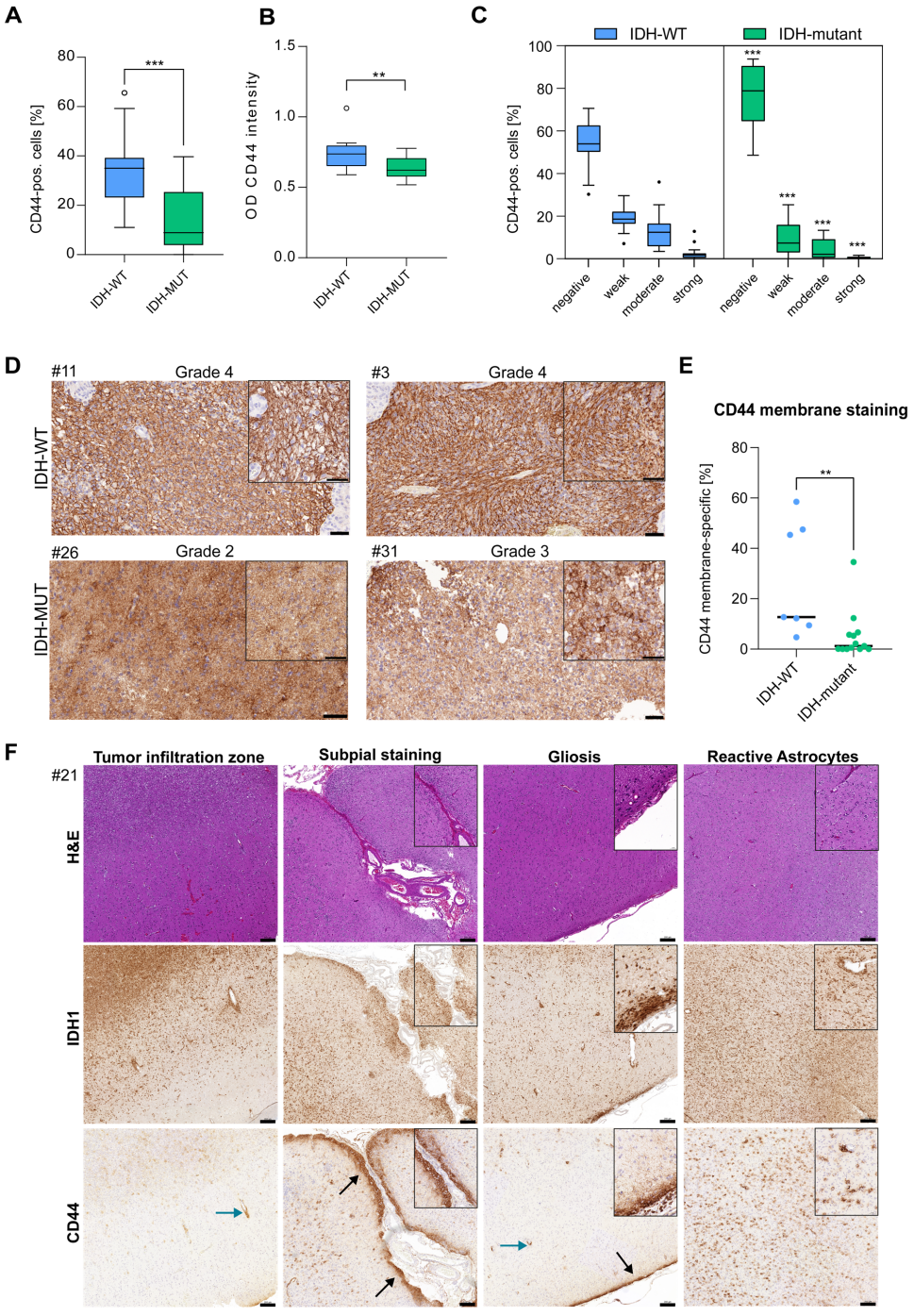

Figure 1. CD44 expression is significantly enriched in membranous regions of IDH WT glioma. (**A**) The percentage of CD44-positive cells was quantified using HALO AI-assisted spatial image analysis of IHC-stained tissue specimens from IDH-wildtype (IDH-WT) ($n = 15$) glioblastoma and IDH-mutated (IDH-MUT) ($n = 17$) astrocytoma tissue specimens. CD44-positive cells are expressed as % of the total cell count. (**B**) CD44 staining intensity was quantified as optical density (OD) in IDH-WT and IDH-MUT tumors. (**C**) CD44 signal intensity was categorized as negative, weak, moderate, and strong in IDH-WT and IDH-MUT glioma. The abundance of cells with each intensity category is expressed as percentage of the total cell count. Statistical significance has been assessed by two-way ANOVA including Sidaks multiple

testing correction. (**D**) Representative CD44-stained tissue sections from two IDH-WT glioblastoma (case #11 and #3) and two IDH-MUT astrocytoma (case #26 and #31) illustrate differences in signal intensity as well as the spatial distribution of CD44 within the tumor tissue. (**E**) An AI-based classifier was trained to identify membrane-specific staining of CD44. The percentage of cells exhibiting membrane-specific CD44 staining was quantified in IDH-WT ($n = 7$) and IDH-MUT ($n = 13$) glioma specimens. (**F**) Representative H&E (upper rows), IDH1 R132H mutation-specific (middle rows) and CD44 (lower rows) stainings illustrating tumor infiltration zone, subpial regions, reactive gliosis and reactive astrocytes in IDH-MUT astrocytoma samples. Scale bars indicate 200 µM. Black arrows indicate subpial CD44 staining or areas of gliosis, whereas turquoise arrows indicate CD44-positive perivascular regions. For statistical evaluation of the results, Shapiro–Wilk test was applied to test for normal distribution. Afterwards statistical significance was calculated by non-parametric *t*-test (**A**,**B**,**E**) or by two way-ANOVA (**C**). Statistical significance levels are given as ** ($p < 0.01$) and *** ($p < 0.001$).

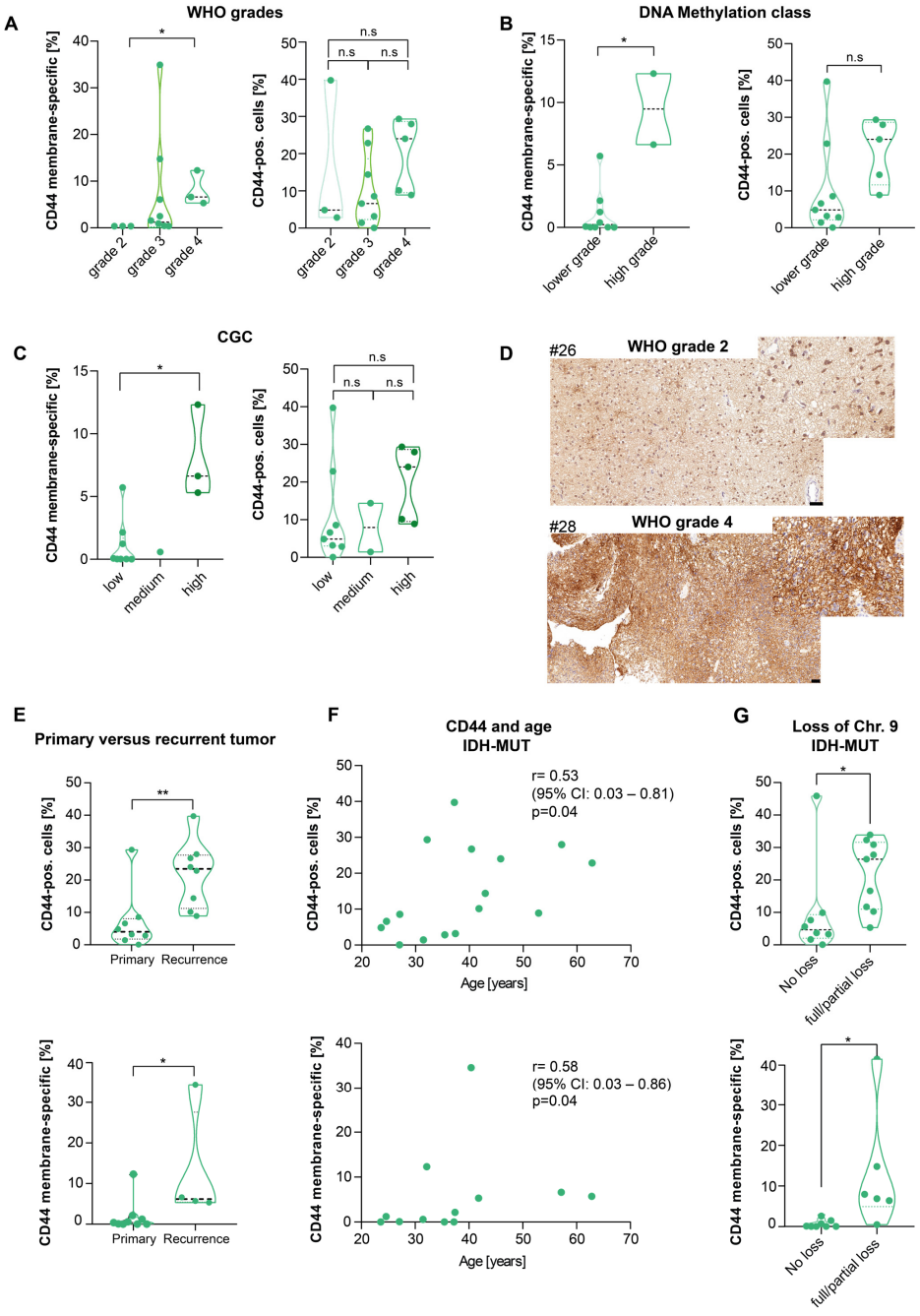

Figure 2. CD44 immunoreactivity increases with tumor progression and adverse clinicopathological features in IDH-mutant glioma. (**A**) CD44 membrane-specific staining (left panel) and percentage of

CD44-positive cells (right) were quantified across histopathological grades 2 ($n = 3$), 3 ($n = 9$), and 4 ($n = 3$) of IDH-MUT astrocytoma. (**B**) CD44 membrane-specific staining (left panel) and percentage of CD44-positive cells (right panel) were quantified in lower- versus high-grade glioma classified according to DNA methylation profiling (MNP classifier). (**C**) CD44 membrane-specific staining (left panel) and percentage of CD44-positive cells (right panel) were compared following application of the DNA methylation-based Continuous Grading Coefficient (CGC) in IDH-MUT tumors stratified into low (<−4.5), medium (−4.5–4.5) and high (>4.5) CGC groups. (**D**) Representative CD44-stained tissue sections of one grade 2 and one grade 4 IDH-MUT astrocytoma are depicted. Scale bars indicate 50 µm. (**E**) CD44 membrane-specific staining (upper panel) and percentage of CD44-positive cells (lower panel) were compared between primary and recurrent IDH-MUT astrocytoma. (**F**) Spearman correlation analyses of the percentage of CD44-positive cells (upper panel) or membrane-specific CD44 staining (lower panel) in relation to patient age at diagnosis are depicted. The corresponding *r* and *p* values from the linear regression analyses are indicated. (**G**) CD44 membrane-specific staining (upper panel) and percentage of CD44-positive cells (lower panel) were analyzed in IDH-MUT astrocytomas according to copy number alterations involving chromosome 9. Tumors were stratified into those with partial or complete loss of chromosome 9 and those without (no loss) chromosome 9 loss. Shapiro–Wilk test was applied to test for normal distribution of the data. Afterwards statistical significance was calculated by Kruskal–Wallis test including Dunn's multiple testing correction (**A**–**C**) or non-parametric *t*-test (**B**,**E**,**G**). Violin plots showing the distribution of individual values, with median (dashed line) and interquartile range (dotted lines). Statistical significance levels are given as * ($p < 0.05$); ** ($p < 0.01$), n.s. = non significant.

In several areas, CD44 staining appeared astrocyte-predominant, with stellate morphology suggestive for reactive astrocytes (Figure 1F, fourth column; Supplementary Figure S1C).

2.2. CD44 Immunoreactivity Increases with Tumor Progression and Adverse Clinicopathological Features in IDH-Mutant Glioma

Prompted by the distinct membranous CD44 staining pattern observed in WHO grade 4 IDH-WT GB and IDH-MUT astrocytoma (compare Figures 1D and 2E), we next quantified CD44 immunoreactivity across histological WHO grades defined by histopathology or DNA methylation profiling. Within our cohort of IDH-MUT astrocytoma comprising WHO grade 2, 3, and 4, membranous CD44 staining was significantly increased in grade 4 tumors, as well as in the combined group of grades 3 and 4 compared with grade 2 astrocytoma (Figure 2A, left panel). Total CD44 immunoreactivity showed a similar but non-significant trend (Figure 2A, right panel). This association was observed irrespective of whether grading was based on histopathology (Figure 2A) or DNA methylation profiling using MNP classifier (Figure 2B), further supporting CD44 as a marker of tumor aggressiveness. To capture the molecular continuum of malignancy beyond conventional histological grading, IDH-MUT astrocytomas were additionally stratified according to the DNA methylation-based continuous grading coefficient (CGC) [27]. Accordingly, only membrane-specific CD44 staining positively correlated with high CGC values (Supplementary Figure S2A; upper and lower panel) and was distinctly increased in the "high-CGC" compared with the "low-CGC" subtype (Figure 2C, Supplementary Table S1).

Representative immunohistochemical staining of an IDH-MUT WHO grade 2 and an IDH-MUT grade 4 astrocytoma illustrate these findings (Figure 2D). Increased malignancy is typically accompanied by enhanced cellular proliferation [28,29]. Accordingly, we confirmed a significantly increased MIB-1 labeling index (percentage of MIB-positive cells) in high-grade IDH-MUT astrocytoma (Supplementary Figure S2B,C, Supplementary Table S1). However, CD44 immunoreactivity (CD44-positive cells and CD44 membrane-specific staining) did not correlate with the percentage of MIB-positive cells (Supplementary Figure S2D, upper and lower panel), suggesting that CD44 reflects biological features of tumor aggressiveness distinct from proliferative activity.

Malignant transformation during tumor progression is another hallmark of glioma biology. Thus, we next compared CD44 protein staining between primary and recurrent gliomas from our cohort of IDH-WT GB and IDH-MUT astrocytomas. Given the already high CD44 levels in IDH-WT tumors, no significant differences were observed between primary and progressed IDH-WT tissues (Supplementary Figure S2E). In contrast, recurrent IDH-MUT astrocytomas exhibited a marked increase in CD44 immunoreactivity, reflected by both overall CD44-positive tumor cells and enhanced membrane-specific staining (Figure 2E, Supplementary Figure S2F). Notably, among the four IDH-MUT WHO grade 2 astrocytoma cases with available follow-up, two progressed to higher-grade lesions following an initial watch-and-wait approach showing prominent membranous CD44 localization, while the remaining two tumors remained stable with almost undetectable membranous CD44 signals (Supplementary Figure S2G). Although these observations are based on a limited number of samples, they provide additional clinical context to our finding. Nevertheless, given the small sample size and the potential influence on subsequent therapeutic interventions, we cannot exclude the impact of treatment on CD44 subcellular localization.

Based on these findings, we aimed to compare CD44 immunoreactivity with well-established clinicopathological parameters. First, our results demonstrate a significant positive correlation between patient age at diagnosis and CD44 positivity (Figure 2F, upper panel) as well as CD44 membranous staining (Figure 2F, lower panel). In addition, loss of chromosome 9, a molecular marker linked to higher-grade gliomas and poor patient outcome in IDH-MUT astrocytoma [30,31], was significantly associated with both CD44 immunoreactivity (Figure 2G, upper panel) and membrane-specific CD44 staining (Figure 2G, lower panel) in IDH-MUT tumors. In contrast, CD44 immunoreactivity did not correlate with other well-established molecular markers of astrocytoma, including *MGMT* promoter methylation (Supplementary Figure S2H, upper and lower panel), chromosome 7q gain (Supplementary Figure S2I), or *ATRX* loss (Supplementary Figure S2J).

2.3. CD44 Immunoreactivity Differs Across Molecular Subclassification in IDH-WT GB

Given the distinct molecular landscape of IDH-WT GB, we next examined whether, in comparison to IDH-MUT astrocytoma, CD44 immunoreactivity is similarly associated with established molecular and clinical characteristics in this tumor entity. According to DNA methylation profiling [6], GB is stratified into three major methylation subclasses: RTK1, RTK2, and MES. Each of these subclasses is associated with distinct alterations, tumor locations, and patient outcomes [32,33]. We therefore investigated whether the percentage of CD44-positive cells and CD44 staining intensity differed among these methylation classes in our IDH-WT GB cohort (Figure 3A,B). Supporting the proposed role of CD44 as a marker of aggressive tumor biology, CD44 immunoreactivity was drastically enhanced in RTK1, which has been associated with poor clinical outcome and frequent *PDGFRA* alterations [16]. Patients with GBs assigned to the mesenchymal methylation class displayed intermediate CD44 staining, while RTK2 tumors exhibited the lowest CD44 immunoreactivity. Representative IHC images of each methylation subclass underline these findings (Figure 3C). Considering patient age as an established prognostic factor in GB, we next examined its relationship with CD44 positivity. Similar to our results in IDH-MUT astrocytoma, CD44 staining positively correlated with patient age in IDH-WT GB (Figure 3D).

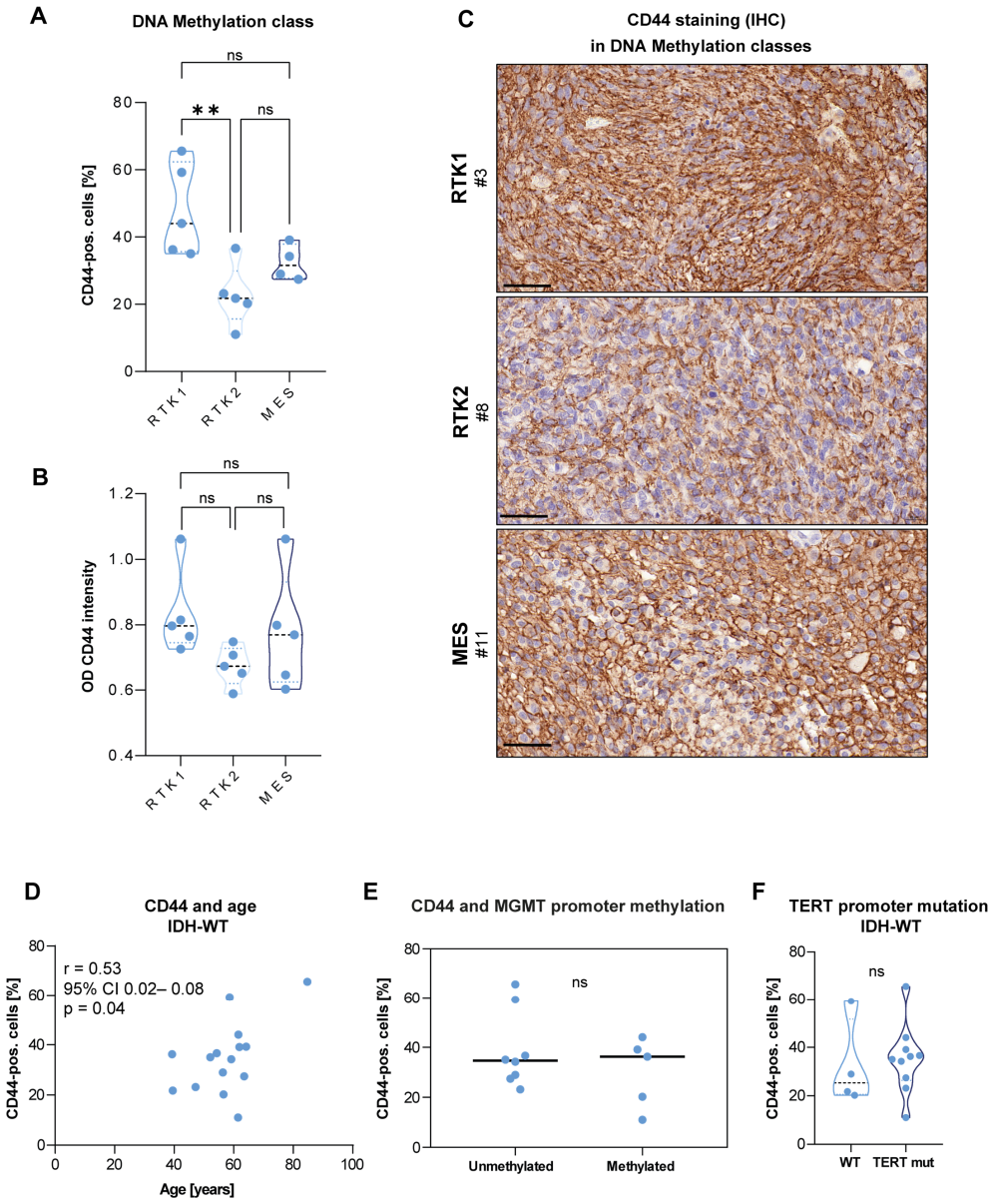

Figure 3. CD44 expression varies across molecular subclasses in IDH-WT GB. (**A**,**B**) CD44-positive cells (**A**) and CD44 staining intensities (**B**) were assessed across DNA methylation subclasses RTK1 (proneural), RTK2 (classical), and MES (mesenchymal) of IDH-WT GB. CD44-positive cells are expressed as a percentage of the total cell count, whereas CD44 staining intensity is represented as optical density (OD) measured across the entire tissue area. (**C**) Representative CD44-stained tissue sections from RTK1, RTK2, and MES subclasses are depicted. Scale bars indicate 50 µm. (**D**) Spearman correlation analysis showing the percentage of CD44-positive cells in relation to patient age at diagnosis are depicted. The R and *p* value from the linear regression analysis is indicated. (**E**,**F**) The percentage of CD44-positive cells was analyzed in IDH-WT GB according to *MGMT* promoter methylation (**E**) or to the *TERT* promoter mutation status (**F**). WT: wildtype. To assess statistical significance, normal distribution of data was assessed by Shapiro–Wilk test. Afterwards statistical significance was calculated by one way-ANOVA (**A**,**B**) or non-parametric *t*-test (**E**,**F**). Violin plots showing the distribution of individual values, with median (dashed line) and interquartile range (dotted lines). Statistical significance levels are given as ** ($p < 0.01$), n.s. = non significant.

Regarding *MGMT* promoter methylation or *TERT* promoter mutation status, no significant differences in CD44 staining between the respective subclasses were observed (Figure 3E,F, Supplementary Figure S3A).

2.4. Spatial Distribution and Cellular Context of CD44 Differ Between IDH-WT and IDH-MUT Glioma

To further characterize the spatial distribution of CD44 in IDH-WT GB and IDH-MUT astrocytoma, we performed multiplex IHC. This approach enables assessment of subcellular localization and the spatial distribution of CD44 together with other glioma-relevant markers within glioma tissue. Consistent with our previous findings from conventional IHC (compare Figure 1E), quantitative analysis of membranous staining by multiplex IHC confirmed significantly higher CD44 immunoreactivity in IDH-WT gliomas ($n = 4$), whereas IDH-MUT astrocytoma ($n = 4$) exhibited weaker and more diffuse CD44 protein expression (Figure 4A).

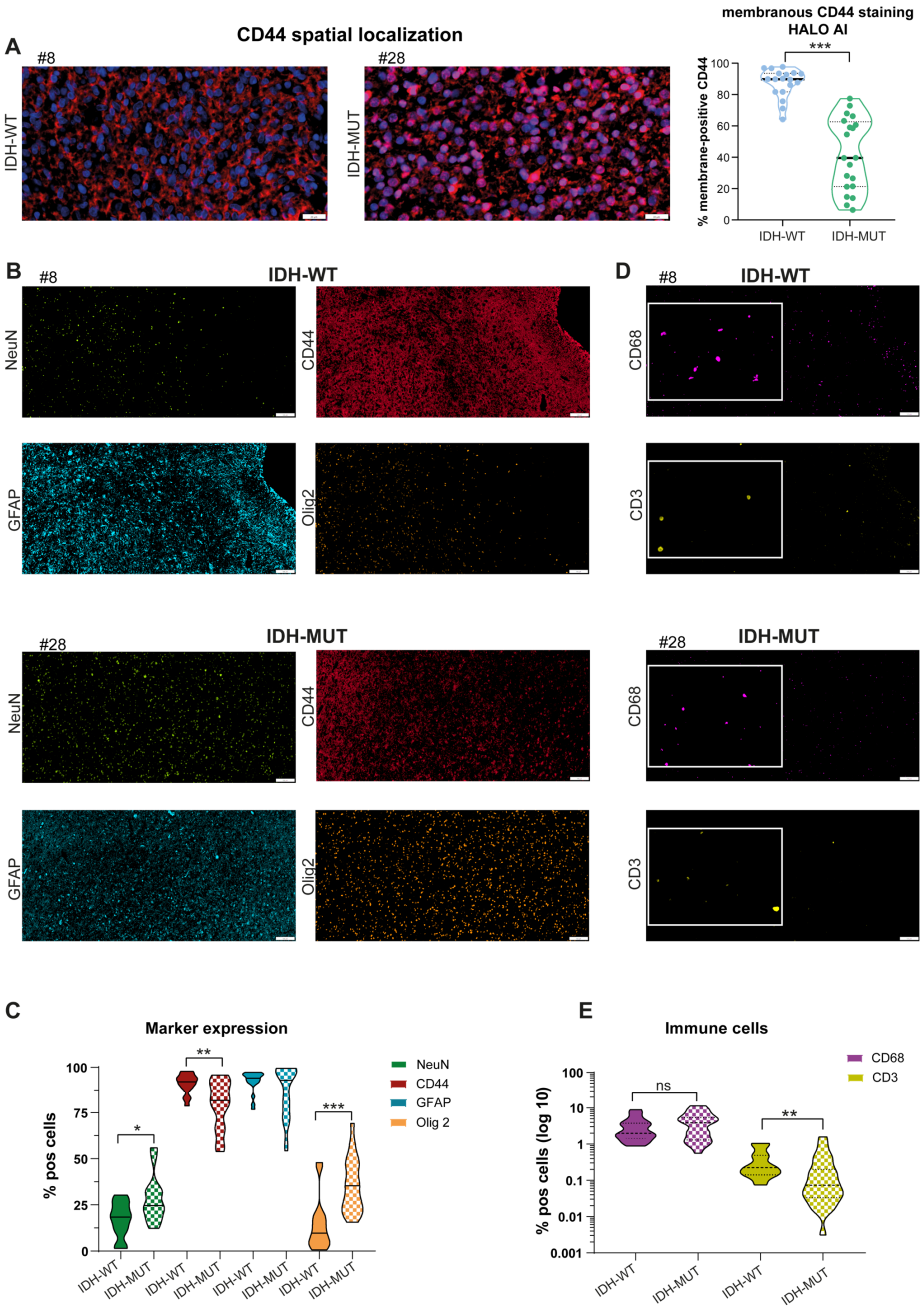

Figure 4. Spatial distribution and cellular context of CD44 differ between IDH-WT and IDH-MUT glioma. Multiplex imaging of IDH-WT ($n = 4$) and IDH-MUT ($n = 4$) tumors was performed to investigate spatial organization. (**A**) Differences in the cellular distribution of CD44

between IDH-WT and IDH-MUT glioma are shown. Representative multiplex IHC images depict CD44 immunofluorescence signals (in red) and nuclei stained with DAPI (blue) of one IDH-WT GB (case #8) and one IDH-MUT astrocytoma (case #28) (left and middle panels). The right panel shows the quantification of membrane-specific CD44 staining across all investigated cases. (**B**) Multiplex IHC of neuronal (NeuN), oligodendroglial (Olig2), and astrocytic (GFAP) lineage markers together with CD44 in IDH-WT (upper panels) and IDH-MUT (lower panels) tumors. Representative images from cases #8 (IDH-WT) and case #28 (IDH-MUT) are shown. (**C**) Quantification of CD44 and glioma-associated lineage markers in IDH-WT ($n = 4$) and IDH-MUT ($n = 4$) tumors was performed using HALO 4.4 software. The number of marker-positive cells are expressed as percentage of total cell number analyzed within regions of interest (ROIs) encompassing the full extent of tumor heterogeneity in each section. (**D**) Immune cell markers (CD68 and CD3) were stained in IDH-WT (upper panels) and IDH-MUT (lower panels) tumors. Representative cases are shown. (**E**) Immune cell infiltration was assessed by immunostaining for the microglial marker CD68 and T-cell-marker CD3. The percentages of marker-positive cells are presented on a log10 scale for better visualization. Statistical differences in marker expression were calculated by *t*-tests comparing IDH-WT and IDH-MUT tumors for each individual marker. Scale bars indicate 100 µM. Violin plots showing the distribution of individual values, with median (dashed line) and interquartile range (dotted lines). Statistical significance levels are given as * ($p < 0.05$); ** ($p < 0.01$) and *** ($p < 0.001$), ns = non significant.

In order to elucidate the cellular composition of both glioma entities and its relationship with CD44, we analyzed the neuronal marker NeuN (*RBFOX3*), the astrocytic marker GFAP, and the oligodendroglial marker Olig2 (Figure 4B; upper and lower panels). Again, our findings demonstrated lower CD44 staining in IDH-MUT astrocytoma compared with IDH-WT GB (Figure 4B,C). In contrast, NeuN- and Olig2-positive cells were significantly more abundant in IDH-mutant astrocytoma, possibly indicating the presence of preserved cortical tissue. GFAP showed a trend toward higher abundance in IDH-WT gliomas, mirroring the distribution of CD44 (Figure 4B,C). Additionally, we examined the immune microenvironment using CD68 and CD3 as markers of microglia/myeloid cells and T-cell infiltration, respectively (Figure 4D, upper and lower panels). The composition of immune infiltrates differed between IDH-WT and IDH-MUT gliomas with microglia being only slightly elevated in IDH-MUT astrocytoma. However, although T-cell infiltration was generally low in both entities, it was significantly reduced in IDH-MUT astrocytoma (Figure 4D,E).

2.5. Integrated Spatial and Transcriptomic Analyses Define CD44-Positive Astrocytic Niches

Given the differences in CD44 and NeuN-positivity between IDH-WT and IDH-MUT gliomas, we further stratified tumors into CD44- and NeuN-high versus -low areas. In parallel, we delineated distinct spatial compartments based on CD44 membrane-specific versus diffuse CD44 staining patterns, which were besides histological features used to distinguish tumor-enriched from non-tumor-enriched areas, respectively.

In line with the analysis of our IHC stainings, membrane-specific CD44 labeling remained significantly lower in IDH-MUT than IDH-WT tumors in both CD44-high and CD44-low regions (Supplementary Figure S4A). Despite this overall difference in CD44 immunoreactivity between IDH-WT GB and IDH-MUT astrocytoma, cells expressing the astrocytic lineage marker GFAP were consistently more abundant in tumor-enriched than in non-tumor-enriched areas, irrespective of the IDH-mutation status (Figure 5A,B). Notably, when investigating CD44-high versus -low expressing regions, significantly elevated levels of the glial marker in IDH-WT GB became apparent (Figure 5A, Supplementary Figure S3B), likely reflecting the higher basal CD44 protein expression in this entity. Furthermore, CD44 and GFAP showed significant spatial co-expression, with higher GFAP levels in CD44-high than in CD44-low regions in both tumor groups (Figure 5C).

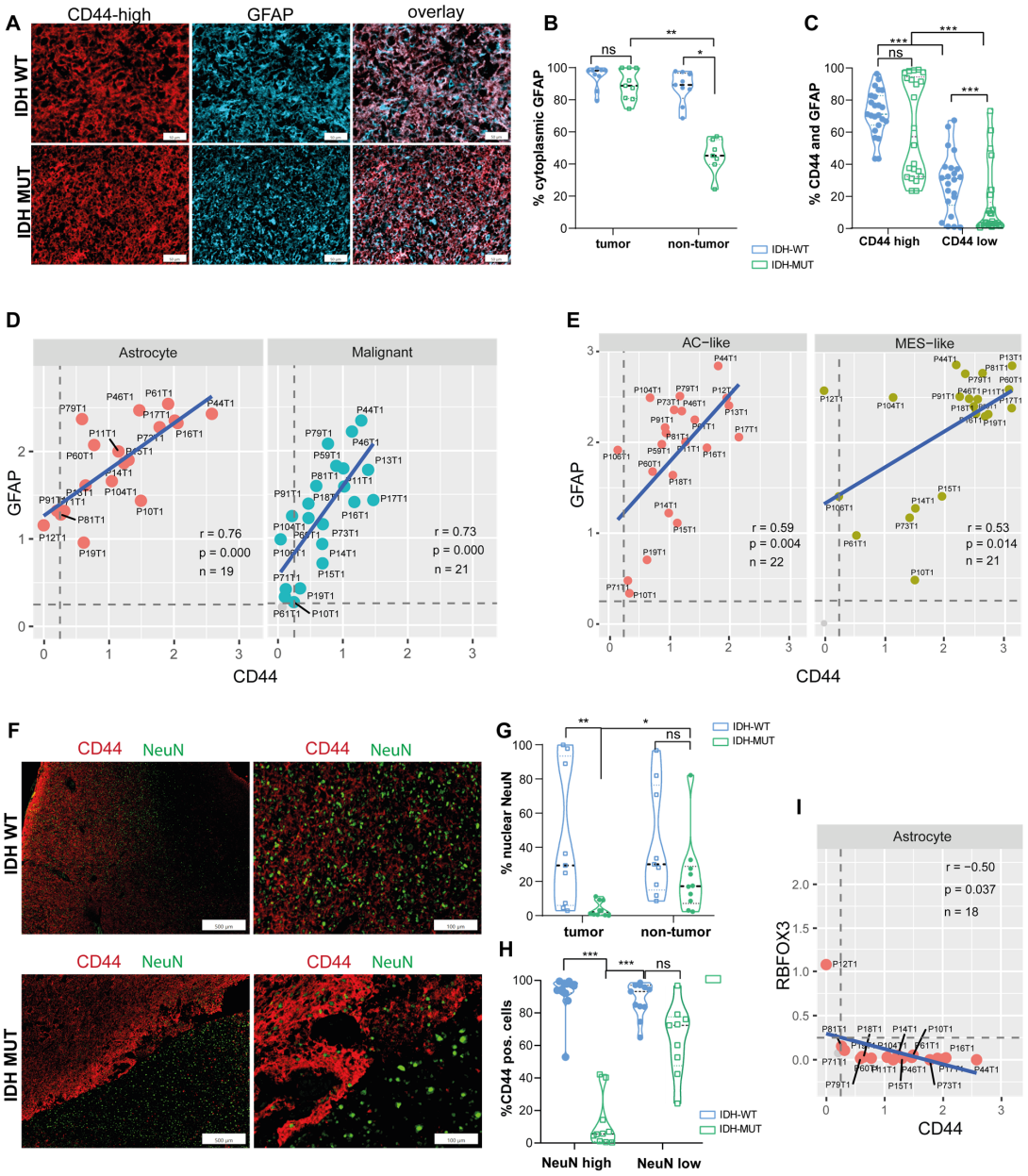

Figure 5. Integrated spatial and transcriptomics analyses define CD44-positive astrocytic niches. (**A**) Representative images of CD44 and GFAP immunostainings in CD44-high regions of IDH-WT and IDH-MUT glioma sections are depicted. Size bars indicate 50 µm. (**B**) Tumor tissue and adjacent non-tumor CNS tissue were delineated based on membranous CD44 staining and corresponding H&E-stained sections. Violin plots show the percentage of GFAP-positive cells in tumor and non-tumor tissue from IDH-WT and IDH-MUT cases. (**C**) Violin plots depict co-expression of CD44 and GFAP in CD44-high versus CD44-low regions across both glioma subtypes. CD44-high and CD44-low regions were delineated based on predefined staining-intensity thresholds in multiplex IHC imaging. Co-expression was quantified using HALO software. (**D**,**E**) Single-nuclei transcriptomic data [17] were analyzed to assess *CD44* and *GFAP* co-expression. Non-malignant astrocytic lineage and malignant cell populations are shown in (**D**). Graphs in (**E**) depict AC-like and MES-like signatures within the malignant cell panel. (**F**) CD44- and NeuN immunofluorescence staining is shown in representative IDH-WT and IDH-MUT tumor tissues. Size bars indicate 500 µm (left) and 100 µm (right): (**G**) Tumor tissue and adjacent non-tumor CNS tissue were delineated based on membranous CD44 staining and corresponding H&E-stained sections. Graph depicts percentage of NeuN-positive cells within cancerous and non-malignant tissue of each glioma subtype. (**H**) Based on staining intensities, tumor tissue was stratified into NeuN-high and NeuN-low regions and analyzed for expression of

the indicated markers in the respective categories. (**I**) Coexpression of *RBFOX3* (NeuN) and *CD44* in astrocytes was additionally assessed using published single nucleus transcriptomic data [17]. Violin plots showing the distribution of individual values, with median (dashed line) and interquartile range (dotted lines). Statistical significances of multiplex images were assessed by one way-ANOVA. Pearson correlation coefficients and statistical significance of single-nuclei transcriptomic data were calculated as described in the methods section. Significance levels are indicated as * ($p < 0.05$); ** ($p < 0.01$) and *** ($p < 0.001$), ns = not significant.

The positive association between CD44 and GFAP protein expression was further validated in IDH-MUT astrocytoma using an independent, recently published single-nucleus RNA-sequencing dataset from the Verhaak group [17]. *CD44* and *GFAP* mRNA levels showed significant positive correlations in both astrocytes and malignant cell populations (Figure 5D; Supplementary Table S4), particularly within malignant AC-like and MES-like cell states (Figure 5E; Supplementary Table S5). Notably, this correlation was significant in the AC-like program of WHO grade 2 IDH-MUT gliomas ($r = 0.82$; $p = 0.044$) but was not retained in higher-grade tumors (Supplementary Table S6). Conversely, higher-grade IDH-MUT tumors were increasingly associated with the MES-like cell state ($r = 0.78$; $p = 0.037$), in which the positive association between *CD44* and *GFAP* remained evident.

In contrast, the neuronal marker NeuN (*RBFOX3*) exhibited an inverse spatial relationship with CD44 expression. This pattern was particularly pronounced in IDH-MUT tumors, where CD44- and NeuN-positive regions were largely spatially segregated (Figure 5F). The neuronal marker NeuN was enriched in non-tumorous regions, predominantly corresponding to cortical tissue, in IDH-MUT tumors, whereas NeuN was more evenly distributed across tumorous and non-malignant CNS tissue of IDH-WT GB (Figure 5G). AI-based quantification further confirmed a significantly lower proportion of CD44-positive cells in NeuN-high compared with NeuN-low regions (Figure 5H). These spatial findings were further supported by the aforementioned sn-RNA-seq datasets [17], demonstrating an inverse correlation between *CD44* and *RBFOX3* expression within the astrocytic cell population (Figure 5I). When integrating all malignant cell states across WHO grade 2, 3, and 4 IDH-MUT astrocytoma, *CD44* expression was positively correlated with *GFAP* but negatively with *RBFOX3* (Supplementary Figure S4C,D). Together, these findings support a spatial and transcriptional association of *CD44* with astrocytic features and AC-like/MES-like malignant cell states, while revealing an opposing relationship with neuronal lineage markers.

3. Discussion

In this study, we investigated the role of the hyaluronic acid receptor CD44 as a potential marker of glioma aggressiveness in both IDH-WT GB and IDH-MUT astrocytoma. Previous analyses of publicly available transcriptomic datasets, including TCGA, have identified elevated *CD44* transcript levels as a predictor of poor overall survival in low-grade gliomas [34]. However, differences in CD44 protein expression, its spatial distribution across glioma subtypes, and its association with other prognostic parameters have not been comprehensively studied. Here, we demonstrate that CD44 protein expression is significantly higher in IDH-WT than IDH-MUT tumors and is predominantly localized to the cell membrane in IDH-WT GB. In contrast, lower-grade IDH-MUT astrocytoma exhibited weaker and more diffuse CD44 staining. Notably, while IDH-WT GB showed high CD44 immunoreactivity already at initial diagnosis, recurrent IDH-MUT tumors displayed a marked increase in both CD44 protein levels and membranous localization. These findings suggest that acquisition of a membrane-associated CD44 phenotype may accompany malignant progression in IDH-MUT astrocytoma. Several mechanisms might contribute to the altered subcellular localization of CD44 in cancer progression, including its retention within lipid

rafts [35] and its association with hyaluronic acid-enriched extracellular matrix (ECM), both of which have been linked to malignant behavior and tumor invasiveness in other cancer types [35,36]. Furthermore, cell-surface CD44 can interact with receptor tyrosine kinases, including EGFR [37,38], thereby modulating downstream signaling pathways involved in tumor cell proliferation, survival and migration, as demonstrated in other malignancies. Whether these interactions contribute to the observed membranous enrichment of CD44 and differ between IDH-MUT astrocytoma and IDH-WT GB remains to be investigated at the cellular level. Given the established involvement of CD44 in tumor invasion, migration, stemness, cellular stiffness and therapy resistance [39–41], its prominent membranous localization in high-grade IDH-WT and IDH-MUT gliomas further supports its potential biological relevance predicting glioma aggressiveness. In line with this, membranous CD44 was significantly enriched not only in recurrent high-grade IDH-MUT, but also in higher-grade astrocytoma defined by histopathological grading or DNA methylation-based classification. Furthermore, membranous CD44 expression correlated with several established adverse prognostic features, including advanced patient age and loss of chromosome 9q, both of which have been linked to more aggressive disease and poorer clinical outcome [31].

Collectively, our findings identify membrane-specific CD44 as a phenotypic feature associated with glioma progression and aggressiveness across molecularly defined glioma subgroups. Importantly, assessing CD44 subcellular localization in addition to overall expression may provide complementary information on tumor biology and potentially improve the identification of tumors with more aggressive characteristics. However, our findings need additional validation in larger clinical cohorts. The prominent cell-surface localization highlights CD44 as an accessible target for therapeutic approaches in high-grade glioma. This includes CAR-T cell therapies (NCT05577091) [42,43] or CD44-mediated uptake of chemotherapy-loaded nanoparticles [44,45]. These findings highlight the potential of membranous CD44 as a therapeutic target, particularly for strategies aiming to improve tumor-selective drug delivery. However, despite promising preclinical findings, and emerging clinical investigations (NCT05577091), the therapeutic potential of CD44-targeting in IDH-WT and IDH-MUT gliomas remains to be established. Our findings therefore highlight the importance of considering not only CD44 expression levels but also its subcellular distribution when evaluating its biological and potential prognostic and therapeutic relevance in gliomas.

Focusing on IDH-WT GB, we discovered distinct differences in CD44 immunoreactivity across the three major DNA-based methylation subclasses, RTK1 (proneural), RTK2 (classical), and MES (mesenchymal). Although CD44 is widely recognized as a hallmark of mesenchymal-differentiated GB [17,46], our finding demonstrate that high CD44 protein expression is not restricted to the MES subgroup. In addition to mesenchymal tumors, RTK1 (proneural) GBs displayed similarly elevated CD44 levels. Together with previous transcriptomic studies showing enrichment of hyaluronic acid-binding genes shaping the extracellular matrix (ECM) organization in proneural GB [47], these findings raise the possibility that CD44 contributes to subtype-specific ECM remodeling. However, the biological and predictive relevance of CD44 as a marker for glioma aggressiveness may be dependent not only on its overall abundance but also on its spatial and subcellular localization. Previous studies have reported an association between perivascular CD44 expression and inferior prognosis, particularly in the proneural subtype, whereas classical and mesenchymal tumors exhibited a more widespread CD44 expression [47,48]. Although our analysis did not specifically assess perivascular CD44 localization, we found enrichment of membranous CD44 across tumor regions in the more aggressive RTK1 and MES methylation subclasses [33,49]. Consistent with previous transcriptomic studies linking *CD44* mRNA levels to patient age in LGG and GB [50], we observed a positive correlation between CD44

expression and age, an established adverse prognostic factor in both IDH-WT GB [51] and IDH-MUT astrocytoma [52]. On the molecular level, *TERT* promoter mutations (*C228T* and *C250T*), contributing to cancer cell immortalization, represent some of the most frequent genetic alterations in IDH-WT GB [53–56]. However, neither *MGMT* promoter methylation nor *TERT* promoter mutation status were significantly associated with CD44 expression in our cohort.

In addition to CD44 immunoreactivity within tumor tissue of high-grade IDH-WT GBs and IDH-MUT astrocytomas, non-neoplastic CNS regions also exhibited a distinct CD44 expression pattern. In particular, reactive astrocytes and perivascular regions showed increased CD44 immunoreactivity. Crosstalk between CD44-expressing reactive astrocytes and glioma stem cells has been proposed as a mechanism promoting stemness and radiation resistance in glioma [57]. In this context, Katz et al. identified CD44 as a marker of reactive astrocytes within perivascular niches of proneural GB and implicated these cells in the maintenance of the glioma stem cell pool [58]. In some cases, we additionally observed fine granular CD44 staining in the surrounding white matter, consistent with reactive gliosis [59], a cellular response to CNS injury or disease. Consistent with our observations, CD44 has also been identified among ECM-associated genes that are altered during reactive astrogliosis [60]. Together, these findings indicate that CD44 expression is not restricted to neoplastic cells but also characterizes specific reactive and perivascular compartments within the glioma microenvironment.

Beyond its association with established molecular parameters of glioma, we aimed to determine how CD44 is spatially organized within the IDH-WT and IDH-MUT tumor microenvironment and how it relates to distinct cellular lineages. NeuN and Olig2, markers associated with neuronal and oligodendroglial lineages, respectively, were more abundant in IDH-MUT than IDH-WT tumors, consistent with a greater representation of non-neoplastic neural tissue in IDH-MUT astrocytomas. Notably, CD44 expression was lowest in cells of oligodendroglial origin, consistent with previous observations by Brown et al. [61]. Although the number of Olig2-positive cells was significantly higher in IDH-MUT than in IDH-WT, this finding should be interpreted with caution due to the limited number of tumors analyzed by multiplex IHC ($n = 4$ IDH-WT and $n = 4$ IDH-MUT).

We next investigated whether the distinct CD44 expression pattern observed between IDH-WT and IDH-MUT gliomas was accompanied by differences in immune infiltration and TME composition. In line with previous studies [62], T-cell infiltration was significantly higher in IDH-WT than in IDH-MUT tumors, whereas microglia abundance did not differ significantly between the two entities. Although increased immune cell infiltration is a recognized feature of IDH-WT GB, the functional state of these immune populations may be shaped by the highly immunosuppressive microenvironment. In contrast, IDH-MUT gliomas have been associated with a more proinflammatory immune milieu, which may contribute to their more favorable clinical course and differential response to immunotherapeutic approaches [63,64]. However, it has to be noted that multiplex IHC analyses were performed in a relatively small subset of tumors ($n = 4$ IDH-WT and $n = 4$ IDH-MUT). Although AI-assisted ROI quantification enables the assessment of multiple regions per specimen, these measurements do not substitute a validation in a larger cohort.

Notably, multiplex IHC revealed a strong spatial association between CD44 and the astrocytic marker GFAP in both IDH-WT and IDH-MUT gliomas, indicating that CD44-positive tumor compartments are enriched for astrocytic features. Complementing protein expression analyses, this positive correlation was independently validated using recently published sn-RNA-Seq data [17] demonstrating a robust positive correlation between *CD44* and *GFAP* expression in both non-malignant astrocytes and malignant cell populations. Notably, this association was most pronounced within the AC-like metaprogram of WHO

grade 2 IDH-MUT gliomas, whereas in higher-grade IDH-MUT tumors *CD44* expression was increasingly associated with MES-like cell states. This shift may reflect changes in tumor cell differentiation during malignant progression and is consistent with current models of glioma evolution, in which lower-grade IDH-MUT astrocytoma progressively acquire mesenchymal features [7,65]. In lower grade IDH-MUT lesions, the pronounced association between CD44 and GFAP may be related to the astrocytic differentiation program, consistent with our IHC observation of prominent CD44 expression in perivascular regions, particularly in astrocytes. In agreement with these findings, Katz et al. identified CD44 as a defining feature of reactive astrocytes and reported profound alterations in astrocytic phenotypes during glioma progression [58]. During malignant transformation, the acquisition of mesenchymal-like features may be accompanied by a loss of astrocytic differentiation markers, including GFAP, as suggested in higher-grade astrocytomas [66]. Conversely, CD44 may become increasingly associated with MES-like programs, potentially reflecting its involvement in hyaluronan-mediated cell–matrix interactions [36]. The increasing contribution of hypoxia-associated spatial organization in higher-grade lesions may further influence these associations [67]. Collectively, these observations suggest that CD44 may accompany a shift from astrocytic differentiation towards more invasive cellular phenotypes during IDH-MUT astrocytoma progression. However, the extent and mechanisms to which these changes reflect altered tumor cell differentiation, changes in cellular composition, and localization or microenvironment interactions remain to be elucidated.

In contrast to the positive correlation between CD44 and GFAP, CD44 and the neuronal marker NeuN (*RBFOX3*) exhibited inverse spatial distribution, particularly in IDH-MUT glioma. While tumor cell compartments were characterized by membranous CD44 expression, the neuronal marker NeuN was predominantly detected in non-neoplastic surrounding CNS tissue and in regions with lower tumor cell infiltration. This spatial segregation was mirrored by transcriptomic data, showing an inverse correlation between *CD44* and *RBFOX3* expression in non-malignant astrocytes, whereas no significant association was observed across malignant cell states [17]. Together with our neuropathological observations, these findings may support the interpretation that this pattern reflects the displacement of native neuronal structures by infiltrating CD44-positive cells into the surrounding cortical tissue. In contrast to IDH-MUT gliomas, IDH-WT GB showed a higher abundance of CD44-positive tumor cells within cortical regions, potentially reflecting the highly infiltrative growth pattern characteristic of this glioma entity.

4. Methods

4.1. Clinicopathological Characteristics of Patient Material

The study cohort comprised tissue specimens from primary and recurrent WHO grade 4 IDH-WT GB (primary: $n = 10$; recurrent: $n = 5$) or WHO grade 2–4 IDH1/2-MUT astrocytoma (primary: $n = 9$; recurrent: $n = 7$). Clinical and molecular characteristics are given in Supplementary Table S1. Patient material was analyzed by conventional histopathological methods, and the majority of samples additionally underwent molecular diagnostic testing. Genome-wide DNA methylation profiling was performed using the Infinium MethylationEPIC BeadChip Kit (Illumina, San Diego, CA, USA) and analyzed with the DKFZ/Heidelberg CNS tumor methylation classifier (versions v11b4 or v12.5). These DNA-methylation profiles were used to calculate a Continuous Grading Coefficient (CGC) for IDH-MUT astrocytoma based on the classification scores described by Ghisai et al. [27]. The resulting CGC values were further stratified into three astrocytoma grade categories: low (CGC < -4.5), medium (CGC -4.5 to 4.5), and high (CGC > 4.5). *TERT* promoter mutation status was determined by RNA sequencing, and *MGMT* promoter methylation was assessed by pyrosequencing using the therascreen ® MGMT Pyro® Kit (QIAGEN, Venlo, The Netherlands).

4.2. Immunohistochemistry (IHC)

For IHC staining, formalin-fixed paraffin embedded (FFPE) tumor tissue slices (2 µm) of IDH-WT GB (n = 15), and IDH-MUT astrocytomas (n = 16) were used. For deparaffinization, slides were incubated in xylol and descending alcohol series before they were steamed for 1 h in EnVision FLEX target retrieval buffer (pH 6) (DAKO by Agilent, Santa Clara, CA, USA) for one hour to expose antigens. After cooling slides and blocking endogenous peroxidases (0.3% H_2O_2), unspecific binding sites were masked by blocking solution (Supplementary Table S2). After washing, primary antibodies were diluted in antibody dilution buffer (Supplementary Table S2) and incubated in a humid chamber at 4 °C overnight. The next day, slides were washed and incubated with EnVision Detection Systems, Rabbit/Mouse (DAKO by Agilent) containing HRP-linked secondary antibodies for 25 min. Subsequently, staining was visualized by using the Peroxidase/DAB system provided with the EnVision Detection System (DAKO by Agilent). Counterstaining was performed in Mayer's hematoxylin before slides were washed and differentiated in hydrochloric acid (0.45%). Finally, tissues were dehydrated in ascending ethanol series and covered with Entelan and coverslips. Slides were scanned using the Pannoramic Scan II Digital Scanner (3DHistech, Budapest, Hungary). Pictures were extracted using CellSens Dimension Desktop software version 4.5 (Evident Scientific, Hamburg, Germany), and staining was quantified using HALO Image Analysis Platform version 4.2.6399 (Indica Labs, Albuquerque, NM, USA) analysis.

4.3. Multiplex IHC

For detection of various antigens within one tumor tissue, multiplex imaging was performed on a set of IDH-WT GB (n = 4) and IDH-MUT astrocytomas (n = 4) using the OPAL 6-Plex Manual detection kit (Akoya Biosciences, Marlborough, MA, USA) following the manufacturer's instructions. To minimize technical variability, all samples were stained simultaneously. Tissue slices (5 µm) were rehydrated and antigens retrieved as described in the previous section. After blocking as recommended by the manufacturer, tissue slices were incubated with the first primary antibody (Supplementary Table S3). Afterwards, secondary antibody OPAL HRP polymer Ms + Rb was incubated for 10 min, before the first OPAL fluorophore was diluted in amplification diluent and incubated for 10 min on tissues covalently binding in the proximity of antibody binding sites. Thereafter, primary and secondary antibodies were stripped away by heating in antigen retrieval buffer while covalently bound fluorescent dyes remained. This procedure allows consecutive binding of different antibodies on the same tissue section and was repeated 4 times until all primary antibodies, and the respective OPAL dyes, were bound to the tissue. Since the last fluorophore (OPAL 780) does not withstand the stripping procedure, it was incubated with TSA-DIG reagent before stripping. Afterwards, tissue was incubated for 45 min with OPAL 780. As a final step, DNA was stained using spectral DAPI, and slices were covered with Diamond Antifade Mountant Media (Thermo Fisher Scientific, Waltham, MA, USA) and coverslips (No. 1.5H) (A. Hartenstein, Würzburg, Germany). Slides were scanned using Evident VS2000, SpectraSplit 7 filter set at 20x. Background subtraction and picture extraction were performed using CellSens Dimension Desktop software version 4.5 (Evident Scientific), and signals were quantified using HALO Image Analysis Platform version 4.2.6399 (Indica Labs). All used antibodies and OPAL dyes are listed in Supplementary Table S3. For image analysis and background subtraction, autofluorescence controls of IDH-WT (n = 2) and IDH-MUT (n = 2) have been included.

4.4. Quantification of IHC and Multiplex Images

HALO Image Analysis Platform version 4.2.6399 (Indica Labs) was used for quantification of IHC ($n = 32$) and multiplex images ($n = 8$). In the case of IHC staining, a tissue classifier was manually trained and used distinguishing tumor tissue from surrounding stroma and unspecific background signals. Tumor and stroma differentiation were additionally confirmed by H&E stainings and in accordance with experienced neuropathologists. Afterwards, another classifier was used for nuclear/cytoplasmic versus membrane identification in order to evaluate CD44 signals in different cellular compartments. Therefore, DAB staining was characterized as membrane stain and a classifier was manually trained to identify regions of membranous localization of CD44. After classification, thresholds for negative, low, intermediate, and high CD44 expression were determined based on DAB signal intensity. In the case of multiplex IHC images classification of tumor and stromal tissues was performed as described before, and thresholds were set for each individual fluorophore distinguishing nuclear/cytoplasmic or membrane location. Thresholds distinguishing weak, moderate, and strong signal intensities were set based on background staining levels observed in autofluorescence controls from IDH-WT ($n = 2$) and IDH-MUT ($n = 2$) tumors. These thresholds were subsequently applied for the quantification of the respective markers. Within each glioma subtype (IDH-WT or IDH-MUT), baselines for the individual Opal intensity signals were each set according to the respective IDH-WT or IDH-MUT autofluorescene controls ($n = 2$ per subtype). Regions of interest (ROIs) ($n = 4$) within each tumor sample ($n = 4$ IDH-WT; $n = 4$ IDH-MUT) were defined either according to CD44 and NeuN staining intensities or according to the pattern of CD44 expression, distinguishing membranous staining in tumor areas from diffuse staining in the surrounding brain parenchyma (e.g., cortex, infiltration zones). For the segmentation of tumor- and infiltration zones, H&E staining and, in the case of IDH-MUT astrocytoma, IDH1 staining was used in accordance with the neuropathological evaluation.

4.5. In Silico Analyses of Single Nuclei Sequencing Data

The single-nucleus RNA sequencing (snRNA-seq) dataset was downloaded from Gene Expression Omnibus (GEO; accession GSE326221; 10x Genomics Single Cell 3′ v3 RNA) [68]. The dataset was restricted to samples annotated by the original authors as IDH-mutated astrocytoma collected at clinical timepoint T1. No additional quality-control filtering was performed because the analysis was based on the processed and annotated dataset provided by the original study. All downstream analyses were performed in R using Seurat (v5.3.1.0) [69]. Pseudobulk expression profiles were generated by summing raw gene counts across all cells belonging to the same biological sample within each cell type and tumor grade using Seurat's AggregateExpression(). Additional pseudobulk profiles were generated using malignant cells only, grouped by tumor grade and malignant cell state. For each cell type and/or tumor grade, pseudobulk observations were included in correlation analyses if the log-normalized expression of either *CD44* or the gene-of-interest exceeded 0.25. Pearson correlation coefficients were calculated between CD44 and gene-of-interest expression using cor.test() from stats (v4.4.0) [70] and visualized with ggplot2 (v4.0.3) [71].

4.6. Statistical Analysis

Data visualization as well as statistical evaluation was performed using Graph Pad Prism v8.0.1. The Shapiro–Wilk test was used to verify normal distribution. In case of a normal distribution of samples, *t*-test or one/two-way ANOVA was used to assess significant differences between two or more groups, respectively. If samples were not normally distributed, we performed the Mann–Whitney U test (non-parametric test) or Kruskal–Wallis

test for comparisons between two or more groups, respectively. For one/two-way ANOVA Dunn's or Tukey's multiple testing correction was applied, respectively. Afterwards, the appropriate statistical test was performed as indicated in the figure legends. Statistical significance levels are given as * ($p < 0.05$); ** ($p < 0.01$) and *** ($p < 0.001$).

5. Conclusions

In summary, our study identified membranous expression of CD44 as potential marker associated with glioma aggressiveness and revealed distinct patterns of CD44 expression and localization between IDH-MUT astrocytoma and IDH-WT GB. Notably, in IDH-MUT astrocytoma, the shift towards MES-like cell states was accompanied by increased membranous CD44 expression, further supporting an association between CD44 and malignant progression in this glioma subtype. From a clinical perspective, assessing CD44 subcellular localization in addition to overall expression may provide complementary information for identifying tumors with more aggressive phenotypic characteristics and could potentially improve risk stratification beyond conventional histopathological and molecular parameters. However, its prognostic relevance, particularly with respect to recurrence and diseases progression, as well as the influence of potential confounding factors need to be established in larger independent cohorts with longitudinal clinical follow-up.

At the biological level, membrane enrichment of CD44 may have important functional implications, as its cell-surface localization facilitates interaction with ECM components including hyaluronic acid [20], fibronectin [72] or osteopontin [57], as well as with receptor tyrosine kinases such as EGFR [37,38]. These interactions can impact cell adhesion, migration and intracellular signaling [21,22], thereby potentially contributing to invasive and aggressive phenotypes. The mechanisms underlying differential membranous CD44 enrichment in IDH-MUT astrocytoma and IDH-WT GB remain to be elucidated. In particular, alternative splicing, post-translational modifications [22], proteolytic processing [23], and altered membrane trafficking [35] may influence CD44 isoform composition, stability and cell-surface retention.

In our previous study, we demonstrated that targeted therapy induces CD44 upregulation in gliomas, accompanied by a mesenchymal cellular transition [73]. Similarly, Gudbergsson at el. reported an increase in CD44 expression following conventional radio/chemotherapy in IDH-WT GB [74]. In the present study, we extended our understanding of CD44 biology by highlighting the importance of its spatial and subcellular distribution, particularly its membranous localization, beyond overall expression levels. Whether therapeutic interventions also promote CD44 redistribution to the cell membrane and whether this is associated with a shift towards mesenchymal differentiation remain important questions for further investigation. An overview of current treatment strategies, their advantages and limitations, and their potential association with subcellular CD44 localization is provided in Supplementary Table S7.

Taken together, our study highlights the importance of considering CD44 localization, rather than overall expression alone, when assessing its biological and potential prognostic relevance in gliomas. In particular, increased membranous CD44 expression in higher-grade IDH-MUT astrocytoma raises the possibility that its subcellular distribution is associated with more aggressive tumor characteristics. However, whether membranous CD44 provides additional prognostic information beyond conventional WHO grading, particularly with respect to recurrence risk and disease progression, remains to be determined. Further studies integrating molecular characterization, treatment history, spatial profiling, and longitudinal clinical outcome data will be essential to elucidate the mechanisms driving CD44 membrane enrichment, establish its independent prognostic values, and explore its potential as a therapeutically actionable target in high-grade gliomas.

Supplementary Materials: The following supporting information can be downloaded at: https://www.mdpi.com/article/10.3390/ijms272210121/s1.

Author Contributions: Conceptualization: C.N.J., W.B. and D.L.; Methodology: C.N.J., L.K., J.F., S.M. and L.P.; Software: C.N.J. and J.F.; Validation: C.N.J., V.Q., T.R.-P. and D.L.; Formal Analysis: C.N.J., L.K., J.F., S.M. and L.P.; Resources (clinical data): K.R., A.S.B., B.K. and G.W.; Writing (Original Draft Preparation): C.N.J., J.F., W.B. and D.L. (with input from all coauthors); Writing—Review and Editing: C.N.J., L.K., V.Q., L.M. (Leah Mager), K.B., L.M. (Laura Marosits), B.R., A.L., L.G.-P., D.K., C.P., T.R.-P., W.B. and D.L.; Visualization: C.N.J. and D.L.; Supervision: W.B. and D.L.; Project Administration: D.L.; Funding Acquisition: C.N.J., W.B. and D.L. All authors have read and agreed to the published version of the manuscript.

Funding: C.N.J. gratefully acknowledges funding from the DOC fellowship of the Austrian Academy of Science (ÖAW). This research was additionally funded in part, by the Austrian Science Fund (FWF) [10.55776/PIN3614424K to D.L.]. Further support was given by the Comprehensive Cancer Research/Initiative Krebsforschung-Grant (to D.L.), the Medical-Scientific Fund of the Mayor of the federal capital Vienna [21165 to D.L.], the FEKF—Fellinger Krebsforschungsverein and the "Forschungsgesellschaft für Cerebrale Tumore" (to D.L.).

Institutional Review Board Statement: This study was performed in line with the principles of the Declaration of Helsinki. Approval was granted by the local Ethics Committee of the Medical University of Vienna (EK No. 1375/2018 and 1616/2020), approval date: 7 December 2018.

Informed Consent Statement: Glioma tissue was collected from 30 patients who underwent surgery at the Department of Neurosurgery at the Medical University of Vienna/General Hospital of Vienna between January 2023 and October 2024. Only cases were included where written informed consent had been obtained.

Data Availability Statement: Single nuclei sequencing data were obtained from publicly available datasets [18].

Acknowledgments: We thank the Imaging facility of the Center for Cancer research for technical assistance regarding imaging experiments.

Conflicts of Interest: Authors state no conflicts of interest relevant for this study.

Abbreviations

ECM	Extracell. Matrix
GCG	Contin. Grading Coeff.
GB	Glioblastoma
MGMT	O-6-Methylguanin-DNA-Methyltransferase
TME	Tumor Microenviron.
TERT	Telomerase Reverse Transcr.
RTK	Recept. Tyrosine Kinase
MES	Mesenchymal
IDH	Isocitrate Dehydrogenase
MUT	Mutant
WT	Wildtype

References

1. Byun, Y.H.; Park, C.K. Classification and Diagnosis of Adult Glioma: A Scoping Review. *Brain Neurorehabilit.* **2022**, *15*, e23. [CrossRef]
2. Park, Y.W.; Vollmuth, P.; Foltyn-Dumitru, M.; Sahm, F.; Ahn, S.S.; Chang, J.H.; Kim, S.H. The 2021 WHO Classification for Gliomas and Implications on Imaging Diagnosis: Part 1-Key Points of the Fifth Edition and Summary of Imaging Findings on Adult-Type Diffuse Gliomas. *J. Magn. Reson. Imaging* **2023**, *58*, 677–689. [CrossRef]
3. Vigneswaran, K.; Neill, S.; Hadjipanayis, C.G. Beyond the World Health Organization grading of infiltrating gliomas: Advances in the molecular genetics of glioma classification. *Ann. Transl. Med.* **2015**, *3*, 95. [CrossRef]

4. Dewangan, S.P.; Narayanan, G.S.; Br, K.K. Analysis of Overall Survival in High-Grade Glioma Patients Treated with Surgery and Adjuvant Therapy. *Cureus* **2025**, *17*, e88792. [CrossRef]
5. Verhaak, R.G.; Hoadley, K.A.; Purdom, E.; Wang, V.; Qi, Y.; Wilkerson, M.D.; Miller, C.R.; Ding, L.; Golub, T.; Mesirov, J.P.; et al. Integrated genomic analysis identifies clinically relevant subtypes of glioblastoma characterized by abnormalities in PDGFRA, IDH1, EGFR, and NF1. *Cancer Cell* **2010**, *17*, 98–110. [CrossRef]
6. Sill, M.; Schrimpf, D.; Patel, A.; Sturm, D.; Jager, N.; Sievers, P.; Schweizer, L.; Banan, R.; Reuss, D.; Suwala, A.; et al. Advancing CNS tumor diagnostics with expanded DNA methylation-based classification. *Cancer Cell* **2026**, *44*, 340–354 e342. [CrossRef]
7. Drexler, R.; Khatri, R.; Schuller, U.; Eckhardt, A.; Ryba, A.; Sauvigny, T.; Duhrsen, L.; Mohme, M.; Ricklefs, T.; Bode, H.; et al. Temporal change of DNA methylation subclasses between matched newly diagnosed and recurrent glioblastoma. *Acta Neuropathol.* **2024**, *147*, 21. [CrossRef]
8. Iluz, A.; Lavi, N.; Charbit, H.; Gutreiman, M.; Idelson, M.; Steiner, D.; Ben-Shushan, E.; Zick, A.; Eden, A.; Mordechai, A.; et al. DNA Methylation-Based Deconvolution Sheds Light on Glioblastoma Heterogeneity and Cell-Type Composition Associated with Patient Survival. *bioRxiv* **2025**. [CrossRef]
9. Solomou, G.; Finch, A.; Asghar, A.; Bardella, C. Mutant IDH in Gliomas: Role in Cancer and Treatment Options. *Cancers* **2023**, *15*, 2883. [CrossRef]
10. Gilbert, M.R.; Liu, Y.; Neltner, J.; Pu, H.; Morris, A.; Sunkara, M.; Pittman, T.; Kyprianou, N.; Horbinski, C. Autophagy and oxidative stress in gliomas with IDH1 mutations. *Acta Neuropathol.* **2014**, *127*, 221–233. [CrossRef]
11. Han, S.; Liu, Y.; Cai, S.J.; Qian, M.; Ding, J.; Larion, M.; Gilbert, M.R.; Yang, C. IDH mutation in glioma: Molecular mechanisms and potential therapeutic targets. *Br. J. Cancer* **2020**, *122*, 1580–1589. [CrossRef]
12. Mellinghoff, I.K.; van den Bent, M.J.; Blumenthal, D.T.; Touat, M.; Peters, K.B.; Clarke, J.; Mendez, J.; Yust-Katz, S.; Welsh, L.; Mason, W.P.; et al. Vorasidenib in IDH1- or IDH2-Mutant Low-Grade Glioma. *N. Engl. J. Med.* **2023**, *389*, 589–601. [CrossRef]
13. Lanman, T.A.; Gonzalez Castro, L.N. Targeting of Mutant Isocitrate Dehydrogenase in Glioma: A Systematic Review. *Cancers* **2025**, *17*, 2630. [CrossRef]
14. Darlix, A.; Preusser, M.; Hervey-Jumper, S.L.; Shih, H.A.; Mandonnet, E.; Taylor, J.W. Who will benefit from vorasidenib? Review of data from the literature and open questions. *Neuro-Oncol. Pract.* **2025**, *12*, i6–i18. [CrossRef]
15. Brito, C.; Azevedo, A.; Esteves, S.; Marques, A.R.; Martins, C.; Costa, I.; Mafra, M.; Bravo Marques, J.M.; Roque, L.; Pojo, M. Clinical insights gained by refining the 2016 WHO classification of diffuse gliomas with: EGFR amplification, TERT mutations, PTEN deletion and MGMT methylation. *BMC Cancer* **2019**, *19*, 968. [CrossRef]
16. Lucchini, S.; Constantinou, M.; Marino, S. Unravelling the mosaic: Epigenetic diversity in glioblastoma. *Mol. Oncol.* **2024**, *18*, 2871–2889. [CrossRef]
17. Johnson, K.C.; Spitzer, A.; Varn, F.S.; Nomura, M.; Garofano, L.; Chowdhury, T.; Lipsa, A.; Zhang, L.; Fernandez, E.C.; Barak, T.; et al. Acquired genetic and cell-state changes in IDH-mutant glioma progression. *Nature* **2026**, *655*, 1048–1059. [CrossRef]
18. Rubio, C.; Perez-Villavicencio, J.; Esteban-Roman, N.F.; Lee, A.; Reyes-Soto, G.; Rubio-Osornio, M. The Extracellular Matrix, the Silent 'Architect' of Glioma. *Biomedicines* **2026**, *14*, 205. [CrossRef]
19. Inoue, A.; Ohnishi, T.; Nishikawa, M.; Ohtsuka, Y.; Kusakabe, K.; Yano, H.; Tanaka, J.; Kunieda, T. A Narrative Review on CD44's Role in Glioblastoma Invasion, Proliferation, and Tumor Recurrence. *Cancers* **2023**, *15*, 4898. [CrossRef]
20. Senbanjo, L.T.; Chellaiah, M.A. CD44: A Multifunctional Cell Surface Adhesion Receptor Is a Regulator of Progression and Metastasis of Cancer Cells. *Front. Cell Dev. Biol.* **2017**, *5*, 18. [CrossRef]
21. Safarians, G.; Sohrabi, A.; Solomon, I.; Xiao, W.; Bastola, S.; Rajput, B.W.; Epperson, M.; Rosenzweig, I.; Tamura, K.; Singer, B.; et al. Glioblastoma Spheroid Invasion through Soft, Brain-Like Matrices Depends on Hyaluronic Acid-CD44 Interactions. *Adv. Healthc. Mater.* **2023**, *12*, e2203143. [CrossRef]
22. Oh, H.J.; Kim, S.T.; Kim, H.J.; Lee, K.T.; Yim, H. Multifaceted roles of CD44 in cancer progression and targeted therapeutic strategies. *Exp. Mol. Med.* **2026**, *58*, 2451–2469. [CrossRef]
23. Okamoto, I.; Kawano, Y.; Murakami, D.; Sasayama, T.; Araki, N.; Miki, T.; Wong, A.J.; Saya, H. Proteolytic release of CD44 intracellular domain and its role in the CD44 signaling pathway. *J. Cell Biol.* **2001**, *155*, 755–762. [CrossRef]
24. Pibuel, M.A.; Poodts, D.; Diaz, M.; Hajos, S.E.; Lompardia, S.L. The scrambled story between hyaluronan and glioblastoma. *J. Biol. Chem.* **2021**, *296*, 100549. [CrossRef]
25. van den Bent, M.J.; Ghisai, S.A.; Wick, W.; Sanson, M.; Brandes, A.A.; Clement, P.M.; Erridge, S.C.; Vogelbaum, M.A.; Nowak, A.K.; Baurain, J.F.; et al. Concurrent and adjuvant temozolomide for 1p/19q non-co-deleted anaplastic glioma (CATNON; EORTC study 26053-22054): Final and exploratory analyses of a randomised, open-label, phase 3 trial. *Lancet Oncol.* **2026**, *27*, 45–56. [CrossRef]
26. Pham, J.; Cote, D.J.; Kang, K.; Briggs, R.G.; Gomez, D.; Prasad, A.; Daggupati, S.; Sisti, J.; Chow, F.; Attenello, F.; et al. Treatment practices and survival outcomes for IDH-wildtype glioblastoma patients according to MGMT promoter methylation status: Insights from the U.S. National Cancer Database. *J. Neurooncol.* **2025**, *172*, 655–665. [CrossRef]

27. Ghisai, S.A.; van Hijfte, L.; Vallentgoed, W.R.; Tesileanu, C.M.S.; de Heer, I.; Kros, J.M.; Sanson, M.; Gorlia, T.; Wick, W.; Vogelbaum, M.A.; et al. Epigenetic landscape reorganisation and reactivation of embryonic development genes are associated with malignancy in IDH-mutant astrocytoma. *Acta Neuropathol.* **2024**, *148*, 50. [CrossRef]
28. Tini, P.; Yavoroska, M.; Mazzei, M.A.; Miracco, C.; Pirtoli, L.; Tomaciello, M.; Marampon, F.; Minniti, G. Low expression of Ki-67/MIB-1 labeling index in IDH wild type glioblastoma predicts prolonged survival independently by MGMT methylation status. *J. Neurooncol.* **2023**, *163*, 339–344. [CrossRef]
29. Krishnan, S.S.; Muthiah, S.; Rao, S.; Salem, S.S.; Madabhushi, V.C.; Mahadevan, A. Mindbomb Homolog-1 Index in the Prognosis of High-Grade Glioma and Its Clinicopathological Correlation. *J. Neurosci. Rural Pract.* **2019**, *10*, 185–193. [CrossRef]
30. Houillier, C.; Mokhtari, K.; Carpentier, C.; Criniere, E.; Marie, Y.; Rousseau, A.; Kaloshi, G.; Dehais, C.; Laffaire, J.; Laigle-Donadey, F.; et al. Chromosome 9p and 10q losses predict unfavorable outcome in low-grade gliomas. *Neuro-Oncology* **2010**, *12*, 2–6. [CrossRef]
31. Huang, T.; Li, S.; Yang, Z.; Liu, J.; Han, Y. Loss of Heterozygosity of 9p Is Associated with Poorer Survival in Patients with Gliomas. *Mol. Neurobiol.* **2016**, *53*, 6407–6412. [CrossRef]
32. Herrmann, T.; Delbridge, C.; Griessmair, M.; Canisius, J.; Mitsdoerffer, M.; Bernhardt, D.; Hostettler, I.C.; Negwer, C.; Yakushev, I.; Meyer, B.; et al. The Spatial Signature of Glioblastoma: A Statistical Re-Assessment of Anatomical Distribution Based on Methylation Subtypes. *Cells* **2026**, *15*, 175. [CrossRef]
33. Kessler, T.; Schrimpf, D.; Doerner, L.; Hai, L.; Kaulen, L.D.; Ito, J.; van den Bent, M.; Taphoorn, M.; Brandes, A.A.; Idbaih, A.; et al. Prognostic Markers of DNA Methylation and Next-Generation Sequencing in Progressive Glioblastoma from the EORTC-26101 Trial. *Clin. Cancer Res.* **2023**, *29*, 3892–3900. [CrossRef]
34. Hou, C.; Ishi, Y.; Motegi, H.; Okamoto, M.; Ou, Y.; Chen, J.; Yamaguchi, S. Overexpression of CD44 is associated with a poor prognosis in grade II/III gliomas. *J. Neurooncol.* **2019**, *145*, 201–210. [CrossRef]
35. Zhang, S.; Zhu, N.; Li, H.F.; Gu, J.; Zhang, C.J.; Liao, D.F.; Qin, L. The lipid rafts in cancer stem cell: A target to eradicate cancer. *Stem Cell Res. Ther.* **2022**, *13*, 432. [CrossRef]
36. Misra, S.; Heldin, P.; Hascall, V.C.; Karamanos, N.K.; Skandalis, S.S.; Markwald, R.R.; Ghatak, S. Hyaluronan-CD44 interactions as potential targets for cancer therapy. *FEBS J.* **2011**, *278*, 1429–1443. [CrossRef]
37. Oh, H.-J.; Min, G.-H.; Kim, D.-E.; Shin, S.-b.; Yim, H. TSG6 promotes epithelial-mesenchymal transition and tumor-associated macrophage polarization through Smad2/3 and MAPK signaling by facilitating TSG6-CD44-TGFβR1 or EGFR complex formation. *Int. J. Biol. Sci.* **2025**, *21*, 4701–4718. [CrossRef]
38. Perez, A.; Neskey, D.M.; Wen, J.; Pereira, L.; Reategui, E.P.; Goodwin, W.J.; Carraway, K.L.; Franzmann, E.J. CD44 interacts with EGFR and promotes head and neck squamous cell carcinoma initiation and progression. *Oral Oncol.* **2013**, *49*, 306–313. [CrossRef]
39. Erhart, F.; Blauensteiner, B.; Zirkovits, G.; Printz, D.; Soukup, K.; Klingenbrunner, S.; Fischhuber, K.; Reitermaier, R.; Halfmann, A.; Lotsch, D.; et al. Gliomasphere marker combinatorics: Multidimensional flow cytometry detects CD44+/CD133+/ITGA6+/CD36+ signature. *J. Cell. Mol. Med.* **2019**, *23*, 281–292. [CrossRef]
40. Mesrati, M.H. Dual-targeting of CD44 and CD133: A promising therapeutic strategy for glioblastoma treatment. *Egypt. J. Neurol. Psychiatry Neurosurg.* **2026**, *62*, 82. [CrossRef]
41. Shmelev, M.E.; Farniev, V.M.; Shved, N.A.; Kumeiko, V.V. Nanomechanical Signatures in Glioma Cells Depend on CD44 Distribution in IDH1 Wild-Type but Not in IDH1R132H Mutant Early-Passage Cultures. *Int. J. Mol. Sci.* **2023**, *24*, 4056. [CrossRef]
42. Zhai, Y.; Li, G.; Jiang, T.; Zhang, W. P12.13.B Locoregional Bi-Specific Car-T Cells Targeting Cd44 and Cd133 in Recurrent Glioblastoma: The First in-Human Clinical Trial Results. *Neuro-Oncology* **2024**, *26*, v69. [CrossRef]
43. Zhai, Y.; Li, G.; Pan, C.; Yu, M.; Hu, H.; Wang, D.; Shi, Z.; Jiang, T.; Zhang, W. The development and potent antitumor efficacy of CD44/CD133 dual-targeting IL7Ralpha-armored CAR-T cells against glioblastoma. *Cancer Lett.* **2025**, *614*, 217541. [CrossRef]
44. Malfanti, A.; Catania, G.; Degros, Q.; Wang, M.; Bausart, M.; Preat, V. Design of Bio-Responsive Hyaluronic Acid-Doxorubicin Conjugates for the Local Treatment of Glioblastoma. *Pharmaceutics* **2022**, *14*, 124. [CrossRef]
45. Kudarha, R.R.; Sawant, K.K. Chondroitin sulfate conjugation facilitates tumor cell internalization of albumin nanoparticles for brain-targeted delivery of temozolomide via CD44 receptor-mediated targeting. *Drug Deliv. Transl. Res.* **2021**, *11*, 1994–2008. [CrossRef]
46. Wang, Y.; Zhou, D.; Hong, Z. Integrative Multi-Omics Analysis Identifies an SPP1-Associated Spatial Mesenchymal-Myeloid Program in Glioblastoma. *Genes* **2026**, *17*, 610. [CrossRef]
47. Rancati, S.; Campolungo, M.; Duarte Dalmolin, G.; Lau, P.; Furia, F.; Coppe, A.; Landuzzi, F.; Vecchi, M.; Cavalli, A.; Gustincich, S.; et al. Molecular subtypes and the (in vitro) response of glioblastoma to temozolomide. *BJC Rep.* **2026**, *4*, 24; Correction in *BJC Rep.* **2026**, *4*, 35. [CrossRef]
48. Xiao, Y.; Yang, K.; Wang, Z.; Zhao, M.; Deng, Y.; Ji, W.; Zou, Y.; Qian, C.; Liu, Y.; Xiao, H.; et al. CD44-Mediated Poor Prognosis in Glioma Is Associated with M2-Polarization of Tumor-Associated Macrophages and Immunosuppression. *Front. Surg.* **2021**, *8*, 775194. [CrossRef]

49. Chehade, G.; Lawson, T.M.; Lelotte, J.; Daoud, L.; Di Perri, D.; Whenham, N.; Duprez, T.; Tajeddine, N.; Tissir, F.; Raftopoulos, C. Long-term survival in patients with IDH-wildtype glioblastoma: Clinical and molecular characteristics. *Acta Neurochir.* **2023**, *165*, 1075–1085. [CrossRef]
50. Du, Z.; Wang, Y.; Liang, J.; Gao, S.; Cai, X.; Yu, Y.; Qi, Z.; Li, J.; Xie, Y.; Wang, Z. Association of glioma CD44 expression with glial dynamics in the tumour microenvironment and patient prognosis. *Comput. Struct. Biotechnol. J.* **2022**, *20*, 5203–5217. [CrossRef]
51. Spiegl-Kreinecker, S.; Lotsch, D.; Ghanim, B.; Pirker, C.; Mohr, T.; Laaber, M.; Weis, S.; Olschowski, A.; Webersinke, G.; Pichler, J.; et al. Prognostic quality of activating TERT promoter mutations in glioblastoma: Interaction with the rs2853669 polymorphism and patient age at diagnosis. *Neuro-Oncology* **2015**, *17*, 1231–1240. [CrossRef]
52. Siddiq, Z.; Gilani, A.; Ung, T.H.; Kleinschmidt-DeMasters, B.K. Isocitrate dehydrogenase-mutant astrocytoma in persons aged 55 years and older: Survival differences versus the young. *J. Neuropathol. Exp. Neurol.* **2025**, *84*, 611–616. [CrossRef]
53. Killela, P.J.; Reitman, Z.J.; Jiao, Y.; Bettegowda, C.; Agrawal, N.; Diaz, L.A.; Friedman, A.H.; Friedman, H.; Gallia, G.L.; Giovanella, B.C.; et al. TERT promoter mutations occur frequently in gliomas and a subset of tumors derived from cells with low rates of self-renewal. *Proc. Natl. Acad. Sci. USA* **2013**, *110*, 6021–6026. [CrossRef]
54. Arita, H.; Yamasaki, K.; Matsushita, Y.; Nakamura, T.; Shimokawa, A.; Takami, H.; Tanaka, S.; Mukasa, A.; Shirahata, M.; Shimizu, S.; et al. A combination of TERT promoter mutation and MGMT methylation status predicts clinically relevant subgroups of newly diagnosed glioblastomas. *Acta Neuropathol. Commun.* **2016**, *4*, 79. [CrossRef]
55. Terzi, N.K.; Yilmaz, I.; Oz, A.B. The Place and Prognostic Value of TERT Promoter Mutation in Molecular Classification in Grade II-III Glial Tumors and Primary Glioblastomas. *Turk. J. Pathol.* **2022**, *38*, 90–98. [CrossRef]
56. Simon, M.; Hosen, I.; Gousias, K.; Rachakonda, S.; Heidenreich, B.; Gessi, M.; Schramm, J.; Hemminki, K.; Waha, A.; Kumar, R. TERT promoter mutations: A novel independent prognostic factor in primary glioblastomas. *Neuro-Oncology* **2015**, *17*, 45–52. [CrossRef]
57. Pietras, A.; Katz, A.M.; Ekstrom, E.J.; Wee, B.; Halliday, J.J.; Pitter, K.L.; Werbeck, J.L.; Amankulor, N.M.; Huse, J.T.; Holland, E.C. Osteopontin-CD44 signaling in the glioma perivascular niche enhances cancer stem cell phenotypes and promotes aggressive tumor growth. *Cell Stem Cell* **2014**, *14*, 357–369. [CrossRef]
58. Katz, A.M.; Amankulor, N.M.; Pitter, K.; Helmy, K.; Squatrito, M.; Holland, E.C. Astrocyte-specific expression patterns associated with the PDGF-induced glioma microenvironment. *PLoS ONE* **2012**, *7*, e32453. [CrossRef]
59. Bolon, B. Toxicologic Pathology Forum Opinion: Interpretation of Gliosis in the Brain and Spinal Cord Observed During Nonclinical Safety Studies. *Toxicol. Pathol.* **2023**, *51*, 68–76. [CrossRef]
60. Zamanian, J.L.; Xu, L.; Foo, L.C.; Nouri, N.; Zhou, L.; Giffard, R.G.; Barres, B.A. Genomic analysis of reactive astrogliosis. *J. Neurosci.* **2012**, *32*, 6391–6410. [CrossRef]
61. Brown, D.V.; Filiz, G.; Daniel, P.M.; Hollande, F.; Dworkin, S.; Amiridis, S.; Kountouri, N.; Ng, W.; Morokoff, A.P.; Mantamadiotis, T. Expression of CD133 and CD44 in glioblastoma stem cells correlates with cell proliferation, phenotype stability and intra-tumor heterogeneity. *PLoS ONE* **2017**, *12*, e0172791. [CrossRef]
62. Berghoff, A.S.; Kiesel, B.; Widhalm, G.; Wilhelm, D.; Rajky, O.; Kurscheid, S.; Kresl, P.; Wohrer, A.; Marosi, C.; Hegi, M.E.; et al. Correlation of immune phenotype with IDH mutation in diffuse glioma. *Neuro-Oncology* **2017**, *19*, 1460–1468. [CrossRef]
63. Kikuchi, M.; Takami, H.; Kobayashi, Y.; Nagaoka, K.; Kitagawa, Y.; Nomura, M.; Takayanagi, S.; Tanaka, S.; Saito, N.; Kakimi, K. Dissecting the Immunological Microenvironment of Glioma Based on IDH Status: Implications for Immunotherapy. *Cells* **2025**, *14*, 1035. [CrossRef]
64. Poon, C.C.; Gordon, P.M.K.; Liu, K.; Yang, R.; Sarkar, S.; Mirzaei, R.; Ahmad, S.T.; Hughes, M.L.; Yong, V.W.; Kelly, J.J.P. Differential microglia and macrophage profiles in human IDH-mutant and -wild type glioblastoma. *Oncotarget* **2019**, *10*, 3129–3143. [CrossRef]
65. Fedele, M.; Cerchia, L.; Pegoraro, S.; Sgarra, R.; Manfioletti, G. Proneural-Mesenchymal Transition: Phenotypic Plasticity to Acquire Multitherapy Resistance in Glioblastoma. *Int. J. Mol. Sci.* **2019**, *20*, 2746. [CrossRef]
66. Sereika, M.; Urbanaviciute, R.; Tamasauskas, A.; Skiriute, D.; Vaitkiene, P. GFAP expression is influenced by astrocytoma grade and rs2070935 polymorphism. *J. Cancer* **2018**, *9*, 4496–4502. [CrossRef]
67. Hoefflin, R.; Greenwald, A.C.; Darnell, N.G.; Mount, C.W.; Tiomkin, Y.; Simkin, D.; Patterson, A.B.; Castro, L.N.G.; Goliand, I.; Golani, O.; et al. Spatial analysis reveals the evolving organization of low-grade and high-grade IDH-mutant glioma. *Cancer Cell* **2026**. [CrossRef]
68. Nomura, M.; Spitzer, A.; Johnson, K.C.; Garofano, L.; Nehar-Belaid, D.; Galili Darnell, N.; Greenwald, A.C.; Bussema, L.; Oh, Y.T.; Varn, F.S.; et al. The multilayered transcriptional architecture of glioblastoma ecosystems. *Nat. Genet.* **2025**, *57*, 1155–1167. [CrossRef]
69. Hao, Y.; Stuart, T.; Kowalski, M.H.; Choudhary, S.; Hoffman, P.; Hartman, A.; Srivastava, A.; Molla, G.; Madad, S.; Fernandez-Granda, C.; et al. Dictionary learning for integrative, multimodal and scalable single-cell analysis. *Nat. Biotechnol.* **2024**, *42*, 293–304. [CrossRef]
70. R Core Team. R: A Language and Environment for Statistical Computing. R Foundation for Statistical Computing, Vienna, Austria. 2024. Available online: https://www.R-project.org/ (accessed on 7 July 2026).

71. Wickham, H. *ggplot2*, 2nd ed.; Use R! Springer: Cham, Switzerland, 2016.
72. McFarlane, S.; McFarlane, C.; Montgomery, N.; Hill, A.; Waugh, D.J.J. CD44-mediated activation of α5β1-integrin, cortactin and paxillin signaling underpins adhesion of basal-like breast cancer cells to endothelium and Fibronectin-enriched matrices. *Oncotarget* **2015**, *6*, 36762–36773. [CrossRef]
73. Mayr, L.; Mager, L.; Gabler-Pamer, L.; Kirchhofer, D.; Freund, J.; Schwark, K.; Lau, B.; Machreich, S.; Senfter, D.; Neumuller, M.; et al. Co-targeting CDK4/6 and MEK reverses mesenchymal transition in therapy-refractory BRAF-altered pediatric high-grade glioma. *J. Exp. Clin. Cancer Res.* **2026**, *45*, 154. [CrossRef]
74. Gudbergsson, J.M.; Christensen, E.; Kostrikov, S.; Moos, T.; Duroux, M.; Kjær, A.; Johnsen, K.B.; Andresen, T.L. Conventional Treatment of Glioblastoma Reveals Persistent CD44+ Subpopulations. *Mol. Neurobiol.* **2020**, *57*, 3943–3955. [CrossRef]

Disclaimer/Publisher's Note: The statements, opinions and data contained in all publications are solely those of the individual author(s) and contributor(s) and not of MDPI and/or the editor(s). MDPI and/or the editor(s) disclaim responsibility for any injury to people or property resulting from any ideas, methods, instructions or products referred to in the content.